Frequency conversion induced by time-space modulated media

Kaijun Yi,[*] Manuel Collet,[†] and Sami Karkar[‡]

LTDS, UMR5513, Ecole Centrale de Lyon, 36 avenue Guy de Collongue, 69130 Ecully, France

Time-space modulated media are realized by periodically modulating parameters of the media in both time and space. In this paper, we study frequency conversion induced by time-space modulated media. Two types of frequency conversion are theoretically and numerically demonstrated; their underlying mechanisms are explained by considering the unusual properties of Bloch modes. We find that the first type of conversion is induced by energy transmission between different orders of Bloch modes, which can be observed when waves inside time-space modulated media are reflected by boundaries. The second type is caused by the Bragg scattering effect occurring inside time-space modulated media; it can be observed when external waves are reflected by time-space modulated media. The frequency can be up or down converted, and the difference caused by the conversion depends on the modulation frequency, which is tunable. Therefore, these frequency conversion phenomena could be exploited to manipulate waves' frequencies for particular purposes.

I. INTRODUCTION

Time-space modulated media are realized by periodically changing parameters of the media both in time and space. The modulation acts like a traveling wave in the media and interacts with medium-supported waves, leading to extraordinary phenomena. Therefore, time-space modulated media have been exploited in many applications. Early examples can be dated back to at least the 1950s. The traveling-wave parametric amplifier was obtained through interactions between two separated circuits and distributed inductances, values of which vary sinusoidally in time and space [1,2]. This kind of application later triggered studies on the electromagnetic wave propagation in time-space modulated media [3–6].

Because of the time-varying feature, time-space modulated media break the reciprocity theorem constraining the physical behavior of media-supported waves [7,8]. Thus, in recent years, time-space modulated media were exploited to realize nonreciprocal wave propagation, which is highly desirable in applications such as acoustic imaging, vibrational energy manipulation, etc. The nonreciprocity can be obtained by interband mode conversion, which is stimulated by moving modulation [9,10]. When the moving modulation is applied in a rotating fashion, the circulator allowing transmission between ports in a unidirectional fashion is realized [8]. Mostly motivated by the possibility of online control of local dynamical properties of mechanical structures [11–13], the elastic wave propagation in time-space modulated structures also has attracted attention [14–16]. It was found that stop bands of the two fundamental Bloch modes in time-space modulated structures can occupy different frequency ranges. Strong nonreciprocal elastic wave propagation was observed within these stop bands.

In this paper, we demonstrate and explain two types of frequency conversion induced by time-space modulated media. The first type can be observed when waves inside the

modulated media are reflected by insulating boundaries of the media; the second can be observed when external waves are reflected by interfaces between homogeneous and modulated media. Note that the second type of frequency conversion was previously roughly discussed by Simon [3] in terms of electromagnetic waves. However, a perturbation method retaining only the fundamental and first-order harmonics was used in his work, which essentially restricts the analysis to very weak modulation and the first stop bands. Our research does not have such restrictions.

To study the frequency conversion, we consider the longitudinal elastic wave in slender beams. We remark here that the governing equation of longitudinal wave in slender beams is a typical equation of a one-dimensional waveguide; therefore, our studies can be easily extended to other types of waves, like electromagnetic waves, acoustic waves, etc. This paper is organized as follows. Section II presents the theories we use. In Sec. II A, we introduce the theory of Bloch modes in time-space modulated beams. Using these Bloch modes, first, the theory of reflection at the ends of time-space modulated beams is developed in Sec. II B, and then the theory of reflection and transmission at interfaces between homogeneous and time-space modulated beams is developed in Sec. II C. The frequency conversion phenomenon is studied in Sec. III using these theories. Section III A is dedicated to demonstrating and explaining the frequency conversion at the ends of time-space modulated beams. Section III B demonstrates and explains the frequency conversion at interfaces between homogeneous and time-space modulated beams. In Sec. IV, we use the finite-element method to verify the theoretically studied frequency conversion phenomenon. Finally, important conclusions of this paper are summarized in Sec. V.

II. THEORY

A. Bloch modes in time-space modulated beams

The beam lying along the x axis in Fig. 1(a) is studied. The density of the beam ρ_0 is constant and homogeneous, while the Young's modulus is modulated in time and space according to

————

[*]kaijun.yi@doctorant.ec-lyon.fr

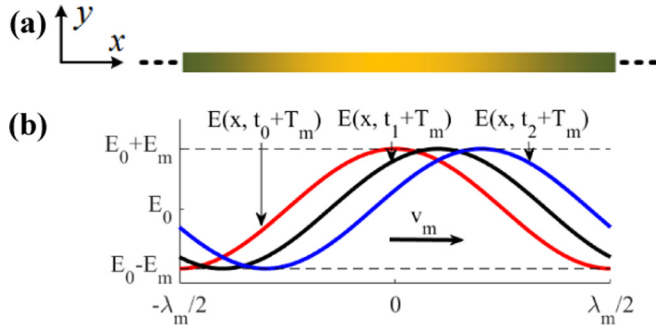[†]manuel.collet@ec-lyon.fr

[‡]sami.karkar@ec-lyon.fr

FIG. 1. (a) A slender modulated beam lying along the x axis. (b) The wavelike time-space modulation of the Young's modulus defined by $E(x,t) = E_0 + E_m \cos(\omega_m t - k_m x)$. The time period is $T_m = 2\pi/\omega_m$, the wavelength (space period) is $\lambda_m = 2\pi/k_m$, and the wave speed is $v_m = \omega_m/k_m$.

a cosine wave function:

$$E(x,t) = E_0 + E_m \cos(\omega_m t - k_m x), \tag{1}$$

where E_0 is the Young's modulus when there is no modulation, E_m is the modulation amplitude, and ω_m and k_m are, respectively, the angular frequency and wave number of the modulation wave, whose wavelength is $\lambda_m = 2\pi/k_m$. The modulation wave propagates along the beam with the speed $v_m = \omega_m/k_m$, as illustrated in Fig. 1(b). In what follows, the modulation expressed in Eq. (1) is described by two dimensionless parameters, namely, the dimensionless modulation amplitude $\alpha_m = E_m/E_0$ and dimensionless modulation speed $\beta_m = v_m/c_0$, where $c_0 = \sqrt{E_0/\rho_0}$ is the phase velocity of the longitudinal wave in a homogeneous beam. The modulation wave could propagate in both directions; $\beta_m > 0$ indicates the wave propagates in the positive direction, and $\beta_m < 0$ means the opposite.

The longitudinal motion $u(x,t)$ in the studied modulated slender beam is governed by

$$\frac{\partial}{\partial x}\left[E(x,t)\frac{\partial u(x,t)}{\partial x}\right] - \rho_0 \frac{\partial^2 u(x,t)}{\partial t^2} = 0. \tag{2}$$

Longitudinal Bloch modes in the modulated beam can be obtained by solving Eq. (2) using the plane-wave expansion (PWE) method as in [15]. The PWE method leads to a quadratic eigenvalue problem (QEP): $\boldsymbol{Q}(\omega,k)\hat{\boldsymbol{U}} = 0$ with a set of $2N + 1$ equations, where N is the truncation order of the harmonics composing a Bloch mode [see Eq. (3)]. The QEP is solved in terms of k by fixing ω, which results in a vector $\boldsymbol{k}$ with $4N + 2$ eigenvalues and a $(2N + 1) \times (4N + 2)$ matrix $\boldsymbol{U}$. Each eigenvalue in $\boldsymbol{k}$ together with the corresponding column in $\boldsymbol{U}$ represents a Bloch mode. Therefore, there are $4N + 2$ longitudinal Bloch modes solved from the QEP.

To describe the Bloch modes in time-space modulated beams well, they are classified into positive-going and negative-going groups according to their group velocities, which are calculated by $c_g = \partial\omega/\partial k$. Bloch modes in each group are organized according to their wave number in an ascending fashion. The nth Bloch modes in the positive-going and negative-going groups are, respectively, represented by u_n^+ and u_n^-, with $n = -N, \ldots, 0, \ldots, +N$. These modes can be
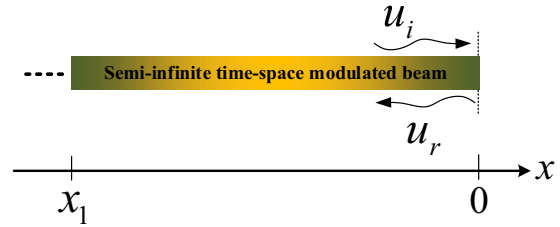

FIG. 2. Reflection at the free end of a semi-infinite time-space modulated beam.

expressed as a group of harmonics:

$$u_n^+(x,t,k_n^+,\omega) = \sum_{q=-N}^{+N} U_{(n,q)}^+ e^{i[(\omega+q\omega_m)t-(k_n^++qk_m)x]},$$

$$u_n^-(x,t,k_n^-,\omega) = \sum_{q=-N}^{+N} U_{(n,q)}^- e^{i[(\omega+q\omega_m)t-(k_n^-+qk_m)x]}, \tag{3}$$

where $k_n^\pm$ are eigenvalues obtained from the QEP and $\{U_{(n,-N)}^+, \ldots, U_{(n,0)}^+, \ldots, U_{(n,+N)}^+\}^T$ and $\{U_{(n,-N)}^-, \ldots, U_{(n,0)}^-, \ldots, U_{(n,+N)}^-\}^T$ are the corresponding eigenvectors.

B. Reflection at the ends of time-space modulated beams

We consider the semi-infinite time-space modulated beam occupying the region $-\infty < x \leqslant 0$, as shown in Fig. 2. The beam end at $x = 0$ is free. Note that one can also apply other kinds of boundary conditions; corresponding results can be obtained using the same process introduced herein.

Assume that waves $u_i(x,t)$ composed of only the $u_0^+(\omega)$ mode are incident on the end:

$$u_i(x,t) = u_0^+ = \sum_{q=-N}^{+N} U_{(0,q)}^+ e^{i[(\omega+q\omega_m)t-(k_0^++qk_m)x]}. \tag{4}$$

The reflected waves $u_r(x,t)$ are represented as the superposition of the negative-going Bloch modes supported by the modulated beam:

$$u_r(x,t) = \sum_{n=-N}^{+N} B_n u_n^-$$

$$= \sum_{n=-N}^{+N} \sum_{q=-N}^{+N} B_n U_{(n,q)}^- e^{i[(\omega+q\omega_m)t-(k_n^-+qk_m)x]}. \tag{5}$$

B_n are contribution coefficients of corresponding Bloch modes.

These waves are constrained by the conservation of momentum at the end:

$$E(0,t)\frac{\partial[u_i(x,t) + u_r(x,t)]}{\partial x}\bigg|_{x=0} = 0. \tag{6}$$

Substituting the expressions for waves [Eqs. (4) and (5)] into Eq. (6) results in

$$\sum_{q=-N}^{+N}\left\{(k_0^++qk_m)U_{(0,q)}^+ + \sum_{n=-N}^{+N}[B_n(k_n^-+qk_m)U_{(n,q)}^-]\right\}$$

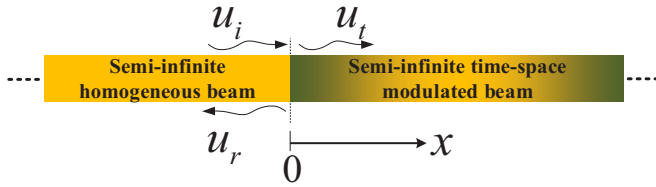$$\times e^{i(\omega+q\omega_m)t} = 0. \tag{7}$$

FIG. 3. Reflection and transmission at the interface between homogeneous and time-space modulated beams.

By exploiting the orthogonality of harmonic functions $e^{i(\omega + q\omega_m)t}$, a set of linear equations is obtained from Eq. (7). Solving these equations, we can obtain the coefficients B_n:

$$\boldsymbol{B} = -\boldsymbol{M}_2^{-1}\boldsymbol{M}_1, \tag{8}$$

where $\boldsymbol{B} = \{B_{-N}, \ldots, B_0, \ldots, B_N\}^T$, $\boldsymbol{M}_1(q + N + 1) = (k_0^+ + qk_m)U_{(0,q)}^+$ with $q = -N, \ldots, 0, \ldots, N$, and $\boldsymbol{M}_2(q + N + 1, n + N + 1) = (k_n^- + qk_m)U_{(n,q)}^-$ with $n, q = -N, \ldots, 0, \ldots, N$.

C. Reflection and transmission at interfaces between homogeneous and time-space modulated beams

Consider that a semi-infinite homogeneous beam (occupying $-\infty < x < 0$) is connected to a semi-infinite modulated beam (occupying $0 \leqslant x < +\infty$) at $x = 0$, as shown in Fig. 3. Young's moduli of these two parts are E_0 and $E(x,t)$ [Eq. (1)], respectively.

Assume that a single harmonic is incident on the modulated beam from the left side:

$$u_i(x,t) = e^{i\omega(t - \frac{x}{c_0})}. \tag{9}$$

The induced waves $u_t(x,t)$ in the modulated beam are represented as the superposition of the positive-going Bloch modes:

$$u_t(x,t) = \sum_{n=-M}^{+M} T_n u_n^+$$

$$= \sum_{n=-M}^{+M} \sum_{q=-M}^{+M} T_n U_{(n,q)}^+ e^{i[(\omega + q\omega_m)t - (k_n^+ + qk_m)x]}, \tag{10}$$

where T_n are contribution coefficients of corresponding Bloch modes and M is the truncation order of Bloch modes in $u_t(x,t)$; the constraint between M and the truncation order N of the QEP will be discussed later.

It can be seen from Eq. (10) that the induced waves inside the modulated beam have harmonic components with frequencies $\omega + q\omega_m$, $q = -M, \ldots, 0, \ldots, M$. Therefore, the reflected waves u_r must be a superposition of harmonics of all possible frequencies $\omega + q\omega_m$:

$$u_r(x,t) = \sum_{q=-M}^{+M} R_q e^{i(\omega + q\omega_m)(t + \frac{x}{c_0})}. \tag{11}$$

R_q are amplitudes of the corresponding harmonics.

These waves are constrained by the continuity of displacement and conservation of momentum at the interface:

$$u_i(0,t) + u_r(0,t) = u_t(0,t),$$

$$E_0 \frac{\partial[u_i(x,t) + u_r(x,t)]}{\partial x}\Big|_{x=0} = E(0,t)\frac{\partial u_t(x,t)}{\partial x}\Big|_{x=0}. \tag{12}$$

Substituting the expressions for waves [Eqs. (9) to (11)] and the two-dimensional Fourier expansion of Young's modulus for the modulated beam [Eq. (1)] into the above continuity conditions,

$$e^{i\omega t} + \sum_{q=-M}^{+M} \left\{ R_q - \sum_{n=-M}^{+M} T_n U_{(n,q)}^+ \right\} e^{i(\omega + q\omega_m)t} = 0,$$

$$-E_0\frac{\omega}{c_0}e^{i\omega t} + \sum_{q=-M}^{+M} \left\{ E_0\frac{\omega + q\omega_m}{c_0}R_q \right.$$

$$\left. + \sum_{n=-M}^{+M}\sum_{p=-1}^{+1} \hat{E}_p[T_n(k_n^+ + (q-p)k_m)U_{(n,q-p)}^+] \right\}$$

$$\times e^{i(\omega + q\omega_m)t} = 0, \tag{13}$$

where $\hat{E}_p$ ($p = -1, 0, 1$) are the Fourier coefficients in the Fourier expansion of the modulated Young's modulus in Eq. (1). $U_{(n,q-p)}^+$ in the second equation in Eq. (13) are elements in the eigenvector $\{U_{(n,-N)}^+, \ldots, U_{(n,0)}^+, \ldots, U_{(n,+N)}^+\}^T$. Therefore, the integral index $q - p$ must satisfy $-N \leqslant q - p \leqslant +N$. Indices q and p satisfy $-M \leqslant q \leqslant M$ and $-1 \leqslant p \leqslant 1$, respectively. Taking all these conditions into account, we have $M \leqslant N - 1$. That's the constraint between M and N mentioned in the above.

Again, by exploiting the orthogonality of harmonic functions $e^{i(\omega + q\omega_m)t}$, the two equations in (13) can be rewritten into the following matrix forms:

$$\boldsymbol{R} - \boldsymbol{M}_3\boldsymbol{T} = -\boldsymbol{I}_1,$$

$$\boldsymbol{M}_4\boldsymbol{R} + \boldsymbol{M}_5\boldsymbol{T} = \boldsymbol{M}_6\boldsymbol{I}_1, \tag{14}$$

where $\boldsymbol{R}$ and $\boldsymbol{T}$ are column vectors containing coefficients R_q and T_n ($n, q = -M, \ldots, 0, \ldots M$), respectively; $\boldsymbol{I}_1$ is a $(2M + 1) \times 1$ vector, in which $\boldsymbol{I}_1(M + 1) = 1$ and other elements are zero; and matrices $\boldsymbol{M}_{(\cdot)}$ are all $(2M + 1) \times (2M + 1)$, whose details are

$$\boldsymbol{M}_3(q + M + 1, n + M + 1) = U_{(n,q)}^+,$$

$$\boldsymbol{M}_4 = \text{diag}(E_0(\omega + q\omega_m)/c_0),$$

$$\boldsymbol{M}_5(q + M + 1, n + M + 1)$$

$$= \sum_{p=-1}^{+1} \hat{E}_p(k_n^+ + (q-p)k_m)U_{(n,q-p)}^+,$$

$$\boldsymbol{M}_6 = E_0\frac{\omega}{c_0}\boldsymbol{I}, \tag{15}$$

where $n, q = -M, \ldots, 0, \ldots, M$ and $\boldsymbol{I}$ is an identity matrix.

Solving Eq. (14), we obtain the coefficients $\boldsymbol{R}$ and $\boldsymbol{T}$. Then using expressions (10) and (11), we have the induced waves inside the modulated beam and the reflected waves.

III. RESULTS

A. Frequency conversion at the ends of time-space modulated beams

In this section, we analyze the frequency conversion induced by reflection at the ends of time-space modulated beams using the theory in Sec. II B. The truncation order used in our simulations is $N = 4$; as will be shown, it is
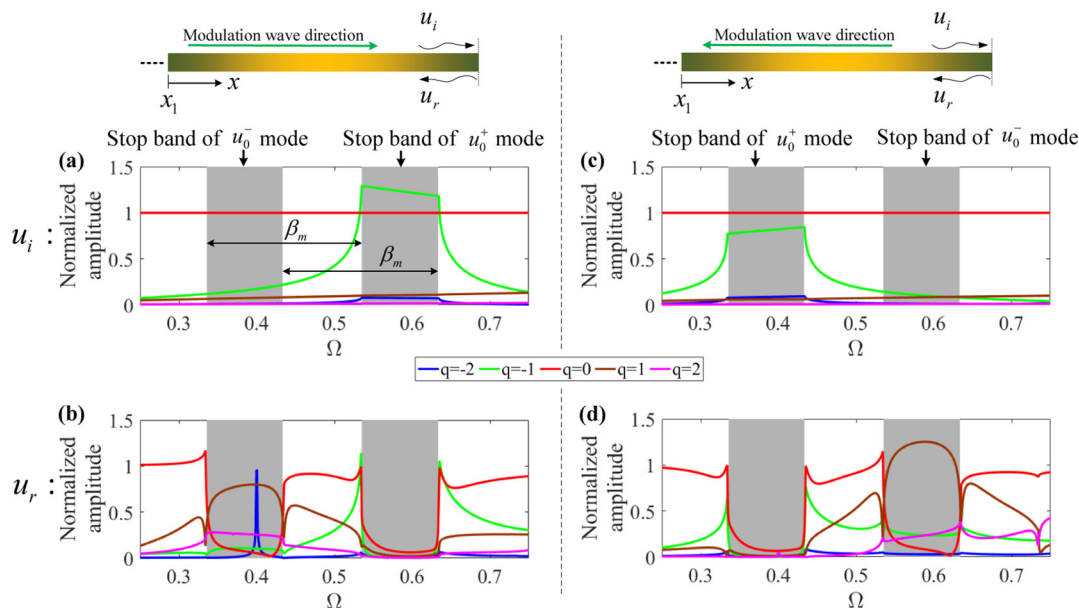
FIG. 4. Case 1: harmonic amplitudes of the (a) incident and (b) reflected waves at $x_1 = -10\lambda_m$ when the modulation wave has parameters $\alpha_m = 0.4$, $\beta_m = 0.2$, propagating in the positive direction. Case 2: harmonic amplitudes of the (c) incident and (d) reflected waves at $x_1 = -10\lambda_m$ when the modulation wave has parameters $\alpha_m = 0.4$, $\beta_m = -0.2$, propagating in the negative direction. Amplitudes in both cases are normalized by the corresponding amplitude $|U_{(0,0)}^+ e^{-ik_0^+ x_1}|$ of the zeroth harmonic of the incident wave. The frequency of the qth harmonic is $\Omega + q\beta_m$.

large enough to take into account all considerable harmonics. We assume that the incident wave $u_i(x,t)$ is from a source at $x_1 = -10\lambda_m$, as shown in Fig. 2. We are concerned with the propagating harmonics among the reflected waves. Therefore, we study the harmonic amplitudes of the incident and reflected waves at x_1, where evanescent waves generated at the end have already significantly decayed. According to Eqs. (4) and (5), at x_1 the qth-harmonic amplitudes of the incident and reflected waves are $|U_{(0,q)}^+ e^{-i(k_0^+ + qk_m)x_1}|$ and $|\sum_{n=-N}^{+N} B_n U_{(n,q)}^- e^{-i(k_n^- + qk_m)x_1}|$, respectively. Figure 4 shows the considerable harmonic amplitudes for two cases. Figures 4(a) and 4(b) show the results of the first case, in which the incident and modulation waves all travel in the positive direction ($\alpha_m = 0.4$, $\beta_m = 0.2$). Figures 4(c) and 4(d) show the results of the second case; the incident wave is positive going, but the modulation wave is negative going in this case ($\alpha_m = 0.4$, $\beta_m = -0.2$). In both cases, amplitudes are normalized by the corresponding amplitude $|U_{(0,0)}^+ e^{-ik_0^+ x_1}|$ of the zeroth harmonic of the incident wave. Note that the dimensionless frequency $\Omega = \lambda_m \omega/(2\pi c_0)$ is used in Fig. 4 and in what follows.

When the incident wave and the modulation wave have the same direction, from Figs. 4(a) and 4(b) we can see that, outside the two stop bands, normally, the dominant harmonic of the reflected wave is coincident with that of the incident wave. Inside the stop band of the u_0^+ mode, the incident harmonics are evanescent; they decay rapidly toward the end. Therefore, reflected harmonic amplitudes at these frequencies are small. Inside the stop band of the u_0^- mode, the incident wave is dominated by the zeroth harmonic. However, the reflected wave is dominated by the first one, the frequency of which is $\Omega + \beta_m$ [because the dimensionless modulation frequency is $\Omega_m = \lambda_m \omega_m/(2\pi c_0) = \beta_m$], inside the stop band of the u_0^+ mode [the

difference between two corresponding frequencies in the stop bands of the u_0^- and u_0^+ modes is β_m, as indicated in Fig. 4(a)]. Therefore, the main frequency is up-converted from the stop band of the u_0^- mode to that of the u_0^+ mode after the reflection. There is an obvious exceptional sharp peak of the amplitude of the negative second harmonic at $\Omega = 0.4$. This peak is caused by the rigid-body motion of the beam because the frequency $(\Omega - 2\beta_m)$ of the negative second harmonic tends to zero as Ω approaches $\Omega = 0.4$. Note that rigid-body motion may occur at other frequencies satisfying $\Omega + q\beta_m = 0$.

Frequency conversion is also observed when the incident wave and the modulation wave have opposite directions. The reverse of the modulation wave direction makes the two stop bands of the u_0^+ and u_0^- modes exchange with each other, as can be seen from Figs. 4(a) and 4(c). Inside the stop band of the u_0^- mode, from Figs. 4(c) and 4(d), we can see that the dominant harmonic is changed from the zeroth to the first after the reflection. In this case we have $\beta_m < 0$, which means the frequency of the first harmonic is $\Omega - |\beta_m|$, inside the stop band of the u_0^+ mode. Therefore, in this case the main frequency is down-converted from the stop band of the u_0^- mode to that of the u_0^+ mode after the reflection.

The cause of the above frequency conversion is explained by further analyzing the components of the reflected waves. Without losing any generality, we choose the modulation parameters to be $\alpha_m = 0.4$, $\beta_m = 0.2$. Figures 5(a) and 5(b) show the components of the incident and reflected waves, respectively, at frequency $\Omega_0 = 0.49$, which is the center between the two stop bands [see Fig. 4(a) or 4(b)]. Figures 5(c) and 5(d) show those at $\Omega_1 = 0.384$, which is the center of the stop band of the u_0^- mode. According to Eqs. (4) and (5), we can see that the incident and reflected waves can be treated both as a group of Bloch modes and as a group of harmonics. These dual properties are shown in Fig. 5. The vertical axis indicates
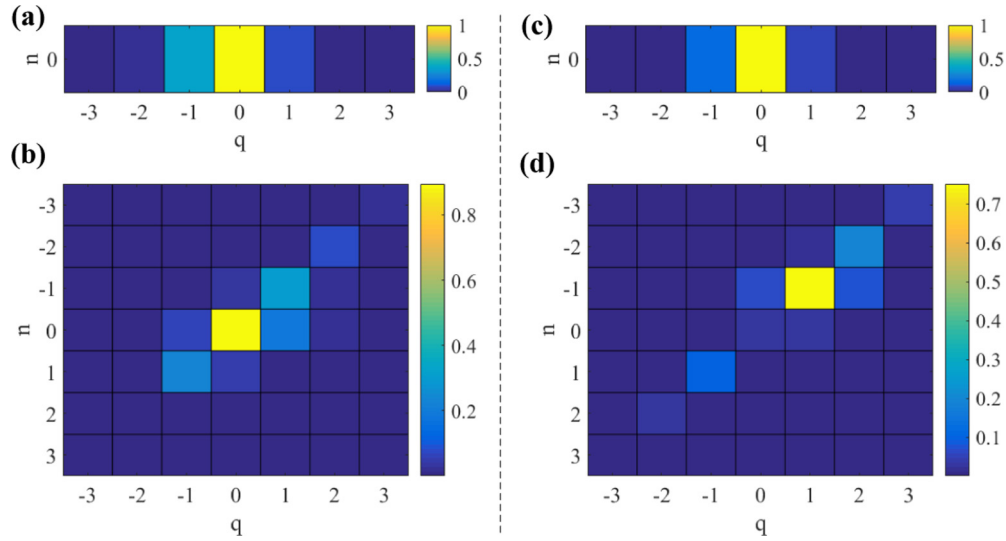
FIG. 5. Components of the (a) incident and (b) reflected waves at $\Omega_0 = 0.49$. Components of the (c) incident and (d) reflected waves at $\Omega_1 = 0.384$. The (n,q) pixel represents the qth harmonic of the nth mode composing the wave, and its color indicates the corresponding amplitude normalized by the amplitude $|U_{(0,0)}^+ e^{-ik_0^+ x_1}|$ of the zeroth harmonic of the incident wave. The modulation parameters are $\alpha_m = 0.4$, $\beta_m = 0.2$.

the orders of Bloch modes [u_n^+ in Figs. 5(a) and 5(c), u_n^- in Figs. 5(b) and 5(d)]; the horizontal one represents the orders of harmonics composing corresponding modes. Therefore, the pixel (n,q) represents the qth harmonic of the nth mode, and its color indicates the corresponding normalized amplitude, which is $|U_{(0,q)}^+ e^{-i(k_0^+ + qk_m)x_1}|/|U_{(0,0)}^+ e^{-ik_0^+ x_1}|$ [see Eq. (4)] in Figs. 5(a) and 5(c) and $|B_n U_{(n,q)}^- e^{-i(k_n^+ + qk_m)x_1}|/|U_{(0,0)}^+ e^{-ik_0^+ x_1}|$ [see Eq. (5)] in Figs. 5(b) and 5(d). From Figs. 5(a) and 5(b) we can see that, when the frequency is outside the stop band of the u_0^- mode, after the reflection, most of the energy is transmitted from the u_0^+ mode to the u_0^- mode, which is dominated by the zeroth harmonic of frequency Ω_0. Accordingly, the main frequency is not converted in this case. However, within the stop band of the u_0^- mode, the reflection makes the energy being transmitted from the u_0^+ mode to the u_{-1}^- mode dominated by the first harmonic have frequency $\Omega_1 + \beta_m$ [Figs. 5(c) and 5(d)]. Therefore, the frequency conversion at the ends of modulated beams

is caused by energy transmission between different orders Bloch modes.

B. Frequency conversion at interfaces between homogeneous and time-space modulated beams

The theory developed in Sec. II C is used to study the frequency conversion at interfaces between homogeneous and time-space modulated beams in this section. The truncation orders are chosen as $N = 5$ and $M = 4$ to take into account all significant harmonics. Assume that a single harmonic $u_i(x,t)$ with frequency Ω is incident on the time-space modulated beam, as shown in Fig. 3. The harmonic amplitudes $|R_q|$ of the reflected waves [see Eq. (11)] at $x = 0$ are shown in Fig. 6. Specifically, Fig. 6(a) shows the results when the incident harmonic and modulation wave have the same direction ($\alpha_m = 0.4$, $\beta_m = 0.2$), and Fig. 6(b) shows the results of the opposite situation ($\alpha_m = 0.4$, $\beta_m = -0.2$). All amplitudes are normalized by the amplitude of the incident harmonic.
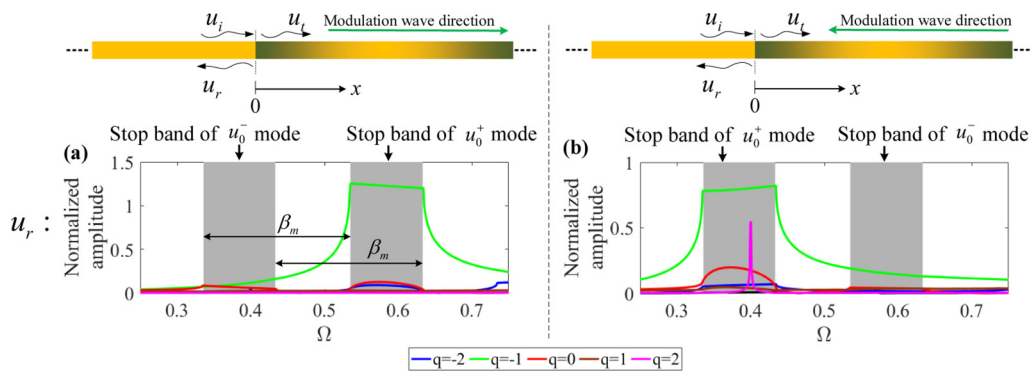

FIG. 6. Harmonic amplitudes of the reflected waves at the interface between a homogeneous beam and a time-space modulated beam. (a) The modulation wave has parameters $\alpha_m = 0.4$, $\beta_m = 0.2$, propagating in the positive direction; (b) the modulation wave has parameters $\alpha_m = 0.4$, $\beta_m = -0.2$, propagating in the negative direction. All amplitudes are normalized by the amplitude of the incident harmonic. The frequency of the qth harmonic is $\Omega + q\beta_m$.
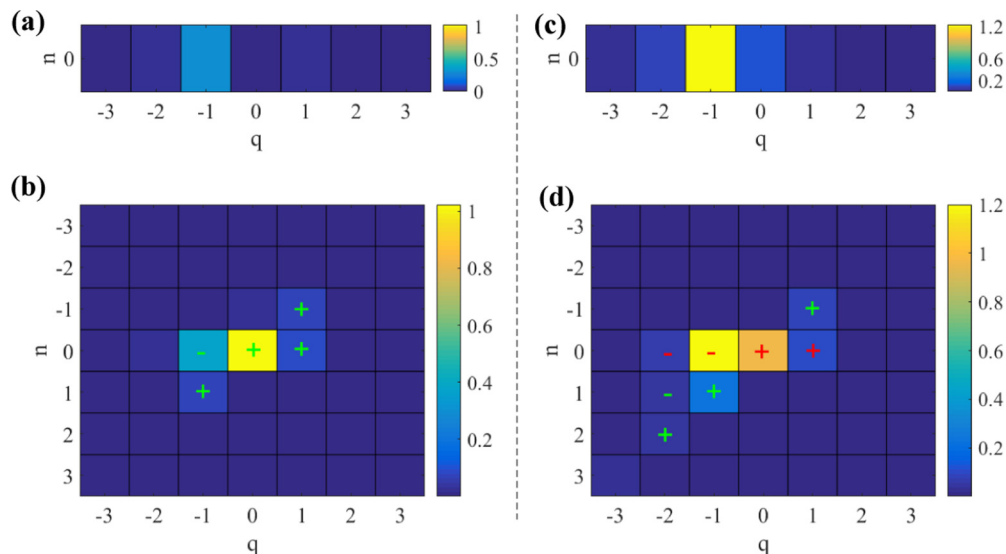
FIG. 7. Components of the (a) reflected waves and (b) induced waves in the modulated beam at $\Omega_0 = 0.49$. Components of the (c) reflected waves and (d) induced waves in the modulated beam at $\Omega_2 = 0.584$. The (n,q) pixel represents the qth harmonic of the nth mode composing the wave, and its color indicates the corresponding amplitude normalized by the amplitude of the incident harmonic. Plus and minus signs indicate positive- and negative-going harmonics, respectively; red and green distinguish evanescent and propagative harmonics. The modulation parameters are $\alpha_m = 0.4$, $\beta_m = 0.2$.

From Fig. 6 we can see that, in both cases at most of the frequencies, the reflected waves are dominated by the negative first harmonic. When the incident harmonic and the modulation wave have the same direction [Fig. 6(a)], the frequency of the negative first harmonic is $\Omega - \beta_m$ $(\beta_m > 0)$, which means the frequency is down-converted after the reflection. On the other hand, when the incident harmonic and the modulation wave have opposite directions [Fig. 6(b)], the negative first harmonic has the frequency $\Omega + |\beta_m|$ $(\beta_m < 0)$. Therefore, in this case the frequency is up-converted. It should be noted that even though the frequency conversion at the interface can be observed at frequencies far from the stop band of the u_0^+ mode when the harmonic is incident on the modulated beam from the left side, the reflected and converted harmonic is a very small part of the incident one. Only in the vicinity of and within the stop band of the u_0^+ mode is the reflection significant, along with the frequency conversion.

To explain the frequency conversion at the interface, the components of the induced waves inside the modulated beam are studied. We choose the modulation parameters to be $\alpha_m = 0.4$, $\beta_m = 0.2$. We perform the simulations at two frequencies. The first one, $\Omega_0 = 0.49$, is the center between the two stop bands in Fig. 6(a), and the second one, $\Omega_2 = 0.584$, is the center of the stop band of the u_0^+ mode. Figure 7 shows the components of the reflected waves and induced waves in the modulated beam at these two frequencies. Like in Fig. 5, in Fig. 7 the pixel (n,q) represents the qth harmonic of the nth Bloch mode [we call the harmonics in the homogeneous beam the zeroth Bloch mode in Figs. 7(a) and 7(c); modes in Figs. 7(b) and 7(d) are u_n^+], and its color indicates the corresponding amplitude, which is $|R_q|$ [see Eq. (11)] in Figs. 7(a) and 7(c) and $|T_n U_{(n,q)}^+|$ [see Eq. (10)] in Figs. 7(b) and 7(d). These amplitudes are normalized by the amplitude of the incident harmonic. There are both positive- and negative-going harmonics in the induced waves; they are indicated by

the plus and minus signs, respectively, in Figs. 7(b) and 7(d). In addition, some of the induced harmonics in Fig. 7(d) [namely, components of the $u_0^+(\Omega_2 = 0.584)$ mode] are evanescent; they are distinguished from the propagative ones by the red and green colors of the plus and minus signs.

Figure 7(b) shows that, at $\Omega_0 = 0.49$, when the harmonic is incident on the interface, most of it is transmitted into the positive-going harmonic $(0,0)$ in the modulated beam with the frequency being unaltered. Also we can see that the negative-going harmonic $(0, -1)$ of frequency $\Omega_0 - \beta_m$ is generated. This harmonic reenters the homogeneous part, consequently leading to the observed frequency conversion. Similarly, at $\Omega_2 = 0.584$, from Fig. 7(d) we can see that the induced waves in the modulated beam is dominated by the harmonics $(0,0)$ and $(0, -1)$, which are evanescent. The harmonic $(0,0)$ is a positive-going harmonic of frequency Ω_2; it rapidly decays inside the modulated beam. On the contrary, the harmonic $(0, -1)$ is a negative-going one of frequency $\Omega_2 - \beta_m$; its amplitude increases toward the interface $x = 0$. The harmonic $(0, -1)$ is transmitted into the homogeneous part, causing the observed frequency conversion.

In both Figs. 7(b) and 7(d), the harmonic $(0, -1)$ can be explained as the reflected positive-going one $(0,0)$ inside the modulated beam. This reflection is caused by the Bragg scattering effect, which must occur at any section of the modulated beam due to the continuous periodic variation of the impedance introduced by the modulation of Young's modulus. Therefore, the frequency conversion observed at the interface is due to the Bragg scattering effect inside the time-space modulated beam.

IV. NUMERICAL SIMULATIONS

The above theoretically studied frequency conversion phenomena are numerically verified by using the finite-element
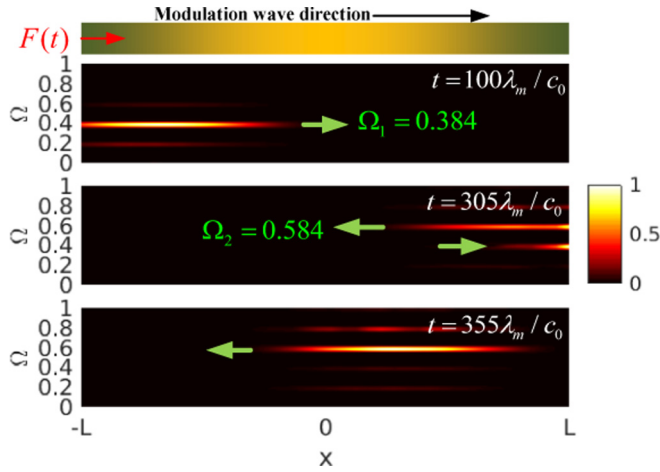
FIG. 8. Frequency conversion at the ends of time-space modulated beams. The modulation parameters are $\alpha_m = 0.4$, $\beta_m = 0.2$. The length of the beam is $2L$, $L = 100\lambda_m$. Both ends of the beam are free. Arrows indicate wave propagation directions.

method in this section. In all the numerical studies, each λ_m length is discretized by 20 two-dimensional Lagrange elements. The generalized α method is used to evaluate the time-domain response; a fixed time step equal to $0.0025\lambda_m/c_0$ is used.

To verify the frequency conversion at the ends, the $2L$ ($L = 100\lambda_m$) long time-space modulated beam shown in the top panel in Fig. 8 is considered. Both ends of the beam are free. The modulation parameters are $\alpha_m = 0.4$, $\beta_m = 0.2$. A narrowband tone burst load centered at $\Omega_1 = 0.384$ (inside the stop band of the u_0^- mode) is applied at the left end along the x direction to generate longitudinal waves. The other three panels show the spectra of waves in the beam at three successive instants; arrows indicate the wave propagation directions. It can be seen that the main frequency of the generated waves is $\Omega_1 = 0.384$ ($t = 100\lambda_m/c_0$). When these
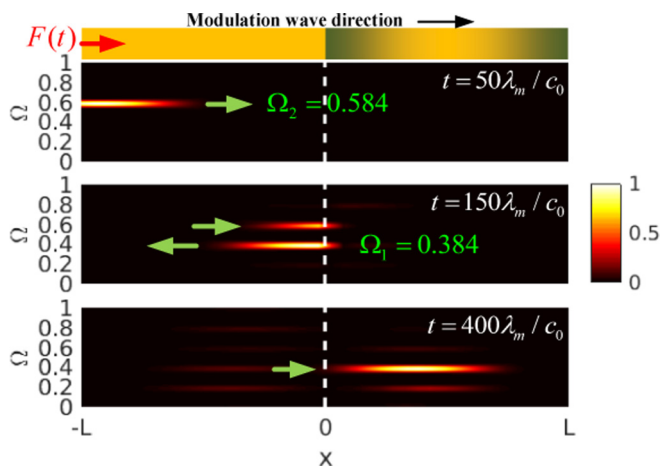
waves are reflected by the right end, the main frequency is up-converted to $\Omega_2 = 0.584$, which is inside the stop band of the u_0^+ mode ($t = 305\lambda_m/c_0$ and $355\lambda_m/c_0$). The frequency difference caused by the conversion is exactly equal to the modulation frequency, which is $\Omega_m = \beta_m = 0.2$, as predicted by the theoretical studies.

The frequency conversion at the interface is verified in Fig. 9. The top panel shows the considered model with both ends free. The left part of the beam ($-L \leqslant x < 0$) has uniform materials, while the right part ($0 \leqslant x \leqslant L$) is a time-space modulated beam with $\alpha_m = 0.4$, $\beta_m = 0.2$. A narrowband tone burst load centered at $\Omega_2 = 0.584$ is applied at the left end to generate longitudinal waves ($t = 50\lambda_m/c_0$). At the interface ($x = 0$), most of these waves are reflected back with down-converted frequency $\Omega_1 = 0.384$ ($t = 150\lambda_m/c_0$). These reflected waves propagate toward the left end and are then reflected back by this static end with unchanged amplitudes and frequencies. Since the main frequencies of these waves are now outside the stop band of the u_0^+ mode, most of them are transmitted into the modulated beam ($t = 400\lambda_m/c_0$).

V. CONCLUSIONS

This paper demonstrated and explained two types of frequency conversion induced by time-space modulated media. The first type is caused by energy transmission between different orders of Bloch modes; it can be observed when interior waves are reflected by boundaries of time-space modulated media. The second type is due to the Bragg scattering effect inside the modulated media; it can be observed when external waves are reflected by time-space modulated media.

The frequency can be up- or down-converted, and the frequency difference is equal to the modulation frequency. In the first type of conversion, when the incident and modulation waves are copropagating, frequency up-conversion is observed after the reflection. On the other hand, frequency down-conversion is observed when the incident and modulation waves are counterpropagating. In the second type, the frequency conversion direction is totally reversed. The copropagating incident and modulation waves lead to frequency down-conversion, and the counterpropagating incident and modulation waves yield frequency up-conversion.

The frequency conversion has significant influences on practical applications of time-space modulated media. It may need to be taken into account in applications using the strong nonreciprocity reported in [15,16]. For example, in approximate infinite or semi-infinite systems, this strong nonreciprocity might be exploited to build unidirectional insulators. However, when the harmonics scattered by the modulated media are considerably reflected back, the one-way energy insulation will fail due to the frequency conversion, as indicated in Fig. 9. Nevertheless, the frequency difference caused by the conversion depends on the modulation frequency (or, say, the modulation speed), which is tunable. Therefore, the frequency conversion could be exploited to manipulate frequencies of waves for particular purposes.

FIG. 9. Frequency conversion at interfaces between homogeneous and time-space modulated beams. The left part of the beam ($-L \leqslant x < 0$) has uniform materials with $\alpha_m = \beta_m = 0$; the right part ($0 \leqslant x \leqslant L$) is a time-space modulated structure with $\alpha_m = 0.4$, $\beta_m = 0.2$, $L = 100\lambda_m$. Both ends of the beam are free. Arrows indicate wave propagation directions.

[1] A. Cullen, Nature (London) **181**, 332 (1958).

[2] P. Tien, J. Appl. Phys. **29**, 1347 (1958).

[3] J. Simon, IRE Trans. Microwave Theory Tech. **8**, 18 (1960).

[4] A. Hessel and A. A. Oliner, IRE Trans. Microwave Theory Tech. **9**, 337 (1961).

[5] E. Cassedy and A. Oliner, Proc. IEEE **51**, 1342 (1963).

[6] E. Cassedy, Proc. IEEE **55**, 1154 (1967).

[7] R. Fleury, D. L. Sounas, M. R. Haberman, and A. Alù, Acoust. Today **11**, 14 (2015).

[8] R. Fleury, D. L. Sounas, and A. Alù, Phys. Rev. B **91**, 174306 (2015).

[9] H. Lira, Z. Yu, S. Fan, and M. Lipson, Phys. Rev. Lett. **109**, 033901 (2012).

[10] M. B. Zanjani, A. R. Davoyan, A. M. Mahmoud, N. Engheta, and J. R. Lukes, Appl. Phys. Lett. **104**, 081905 (2014).

[11] Y. Y. Chen, R. Zhu, M. V. Barnhart, and G. L. Huang, Sci. Rep. **6**, 1 (2016).

[12] Y. Fan, M. Collet, M. Ichchou, L. Li, O. Bareille, and Z. Dimitrijevic, Smart Mater. Struct. **25**, 055032 (2016).

[13] K. Yi, M. Collet, M. Ichchou, and L. Li, Smart Mater. Struct. **25**, 075007 (2016).

[14] N. Swinteck, S. Matsuo, K. Runge, J. O. Vasseur, P. Lucas, and P. A. Deymier, J. Appl. Phys. **118**, 063103 (2015).

[15] G. Trainiti and M. Ruzzene, New J. Phys. **18**, 083047 (2016).

[16] H. Nassar, X. C. Xu, A. N. Norris, and G. L. Huang, J. Mech. Phys. Solids **101**, 10 (2017).